Performance assessment of an improved gasifier stove using biomass pellets: An experimental and numerical investigation

Himanshu, Kurmi, O. P., Jain, S. & Tyagi, S. K.

Original citation & hyperlink:
Himanshu, , Kurmi, OP, Jain, S & Tyagi, SK 2022, 'Performance assessment of an improved gasifier stove using biomass pellets: An experimental and numerical investigation', *Sustainable Energy Technologies and Assessments*, vol. 53, no. Part A, 102432.
https://dx.doi.org/10.1016/j.seta.2022.102432

DOI 10.1016/j.seta.2022.102432
ISSN 2213-1388
ESSN 2213-1396

Publisher: Elsevier

Performance assessment of an improved gasifier stove using biomass pellets: An experimental and numerical investigation

Himanshu[a], O. P. Kurmi[b], Sanjeev Jain[c] and S. K. Tyagi[a*]

a. Department of Energy Science and Engineering, Indian Institute of Technology Delhi, Hauz Khas, New Delhi 110016, India
b. Faculty Research Centre for Intelligent Healthcare, Coventry University, Coventry CV1 5FB, United Kingdom
c. Department of Mechanical Engineering, Indian Institute of Technology Delhi, Hauz Khas, New Delhi 110016, India

Abstract

This article presents an experimental and computational study of a forced draft cookstove having separate primary and secondary air fans, while utilizing pellets as fuel. A two-dimensional axisymmetric computational fluid dynamics model of the developed cookstove has been created in ANSYS Fluent to analyze the fluid flow, temperature distribution and heat loss from the different parts of the cookstove. The simulation results showed that more than one fourth of the total heat produced by the burning of fuel was being lost to the ambient environment through the outermost wall of cookstove. Also, the temperature of the outer wall of the cookstove was found to be higher than the temperature of secondary air being preheated in the annulus chamber. Therefore, the developed model was further modified by using glass wool insulation which resulted in an increment of 5.7% in thermal efficiency, while the emissions of CO and $PM_{2.5}$ were reduced by 7.1% and 25.9%, respectively. The performance of the developed models have also been compared with other pellet based forced draft models available globally, and the thermal efficiency of the Mimi Moto cookstove was found to be highest followed by FD 2.2 model.

Keywords: Forced draft; Pellets; Thermal performance; Emission reduction potential; Heat loss.

[*] Corresponding author: Email: sudhirtyagi@yahoo.com

1 Introduction

Globally, more than 2.6 billion people lack access to clean cooking facilities, and one-third of the world's population utilizes solid fuel to fulfil their energy requirements for cooking and/or heating purposes (IEA, 2020). Despite improved socioeconomic status for much of the world population, the absolute number of individuals exposed to smoke from burning solid fuel has remained about the same over the past 3-4 decades (Bonjour et al., 2013). The inefficient burning of biomass leads to a higher level of household air pollution (HAP), such as emissions of elemental carbon, organic carbon, particulate matter ≤2.5 micrometers in aerodynamic diameter ($PM_{2.5}$), carbon monoxide (CO) and polyaromatic hydrocarbons (Kim et al. 2011, Pandey et al. 2017). Both short- and long-term exposure to these emissions is associated with increased risk of respiratory and cardiovascular diseases, lung cancer, and weakened immune system, especially in women and children, as women perform cooking activities in most of the low- and middle-income countries (LMICs), while accompanying their children (Smith et al., 2014, Zhang and Smith, 2017, Rajkumar et al. 2019). Globally, more than 2.5 million deaths are attributed to smoke released from cooking related activities while meeting the cooking energy demand (IEA, 2020). Currently, many researchers are working to develop a reliable, highly efficient cookstove with low emissions of airborne pollutants (Birzer et al., 2013, Tryner et al., 2016, Tryner et al., 2018, Tyagi 2022).

The forced draft cookstoves are a promising design as they can improve thermal efficiency while reducing CO and $PM_{2.5}$ (MacCarty et al., 2010, Sharma and Dasappa, 2017, Himanshu et al., 2021). The secondary air supply above the fuel bed in forced draft cookstoves has improved air mixing with volatiles and reduced $PM_{2.5}$ emissions (Jetter et al., 2012, Kirch et al., 2018)). Several experimental studies have been carried out to investigate the performance of forced draft cookstoves having primary and/or secondary air supplies with different configurations (Tryner et al., 2014, Chen et al., 2016). The effect of secondary air injection in a wood-burning cookstove has been studied, and the results indicated that the secondary air strongly influenced the emission of particulate matter (Kirch et al., 2016, Caubel et al., 2018). It has been observed that the increased airflow rates of secondary air may result in the quenching of flame, which in turn can increase the emission of fine particles (Caubel et al., 2018). Further, the air injection may lower the total mass of the particulate matter; however, it may increase the concentration of total ultrafine particles (Rapp et al., 2016). Therefore, optimizing the air supply to the forced draft cookstoves is essential for a particular design.

There is a lack of standard procedure required for the development of improved cookstoves in the literature (Arora and Jain, 2016, Obeng et al., 2021). Therefore, the majority of the cookstoves are designed through an iterative process, which is time consuming as prototypes are designed, tested and then stove parameters are refined to conform with the internationally accepted cookstove testing protocols (MacCarty and Bryden, 2015). Computational fluid dynamics (CFD) is a powerful tool that can be used cost-effectively while saving resources and time, for detailed analysis of the systems involving fluid flow, combustion, and heat transfer. Several authors have used CFD simulations to understand the physical processes occurring during the burning of fuel inside the cookstove to get insight into the operating parameters that affect the performance of the cookstove (Ali and Wei, 2017, Husain et al., 2019). A steady-state CFD model was developed to investigate the effect of inlet air ratio on the performance of a natural draft cookstove utilizing biomass as fuel (Pande et al., 2020). The extensive literature suggested that the CFD approach was not used to calculate the heat loss from forced draft cookstoves. Also, the secondary air domain has not been modelled in any computational study to investigate the fluid flow behaviour in these cookstoves.

In the present study, a forced draft cookstove model named FD2.1 has been designed. Its performance has been investigated experimentally using Bureau of Indian Standards (BIS) test protocol (BIS, 2013). The primary and secondary airflow rates to the developed cookstove have also been optimized using a regulated dc voltage supply to achieve the higher values of flame temperature in the combustion zone below the bottom of the cooking vessel. Further, the developed cookstove has been modelled in ANSYS Fluent to analyze the fluid flow, combustion and heat transfer mechanism. The developed model has also been modified based on heat loss calculated through the computational results. The performance parameters, such as the thermal efficiency and the emissions of CO and $PM_{2.5}$, of the modified cookstove have also been compared with those of the developed model. Further, annual emissions and their reduction potentials have been estimated compared to the traditional cookstoves using different solid fuels.

2 Materials and methods

The forced draft cookstove utilizing biomass as fuel was designed, developed, and tested at the Indian Institute of Technology Delhi. The basic design principles and the methodology followed for evaluating the different parameters of a gasifier based cookstove model were adopted from published literature (Bolenio, 2005, Pal et al., 2016, Gupta et al., 2020). The various design parameters of the developed cookstove model were calculated as follows:

2.1 Power output (Q_n)

The power output, also termed as cooking power, is the amount of heat produced/supplied from a cookstove to cook a particular amount of food or to heat/boil a particular amount of water. This depends on the quantity and specific heat of food to be cooked for particular cooking activity. According to the National Advisory Board on Energy, the amount of useful energy derived from biomass to cook food was estimated to be 2.6 MJ per capita in rural India and the same is taken as the basis in the present study (Srivastava et al., 2012). The current model was designed to cook food for a family of 8-10 people, and therefore, the required power output was calculated as 2.5 KW.

2.2 Fuel consumption rate (FCR)

Fuel consumption rate refers to the amount of fuel consumed per hour in the cookstove and it may also be defined as the amount of fuel fed to the cookstove per unit time. This depends on the power output (Q_n), calorific value (CV_f) of biomass fuel, thermal efficiency (η) of the cookstove and can be calculated using the following formula (Gupta et al., 2020, Himanshu et al., 2021):

$$\mathrm{FCR} = \frac{Q_n}{CV_f \times \eta}, \text{ (kg/hr)} \tag{1}$$

2.3 Combustion chamber diameter (D)

The diameter of the combustion chamber refers to the cross-section of the chamber in which fuel is burnt during combustion. It is one of the important parameters that need to be decided carefully to achieve high-performance in terms of thermal efficiency and emission characteristics for an appropriate power level. The diameter of the combustion chamber impacts the fuel consumption rate (FCR, kg/h), specific gasification rate of the fuel biomass (SGR, kg/m^2-h), and it can be estimated for certain types of stoves using the following formula (Gupta et al., 2020, Himanshu et al., 2021):

$$D = \left(\frac{1.27 \times FCR}{SGR}\right)^{0.5}, (m) \tag{2}$$

SGR is the specific gasification rate of biomass, (SGR of wood = 90 kg/m^2-hr) (Chendake et al., 2014).

2.4 Height (H)

This indicates the combustion chamber's height and the distance between the bottom and top end. The diameter and height of the combustion chamber are the two most important design parameters as they collectively decide the amount of fuel that can be filled in the cookstove. The height of the combustion chamber impacts the bulk density of fuel (ρ_f, kg/m^3), time (t, h) required for burning of each batch of fuel loaded into the combustion chamber of the stove and specific gasification rate of biomass, and can be computed by using the following equation (Gupta et al., 2020, Himanshu et al., 2021):

$$H = \frac{SGR \times t}{\rho_f}, (m) \tag{3}$$

2.5 Air flow rate (AFR)

This is the flow rate of the air that needs to be supplied into the combustion chamber for nearly complete combustion of the fuel. Air flow rate depends on the density of air (ρ_a, kg/m^3), fuel consumption rate (FCR, kg/h), stochiometric air requirement (SA, kg of air/kg of fuel) and equivalence ratio (ε), and can be computed from the following empirical formula (Chendake et al., 2014):

$$AFR = \frac{\varepsilon \times FCR \times SA}{\rho_a}, (m^3/h) \tag{4}$$

A schematic of the cookstove designed and tested is shown in Fig. 1a. The stove consists of two concentric cylinders, namely the inner cylinder and outer cylinder, each having diameters of 140 mm and 180 mm, respectively. The height of the inner cylinder is 300 mm, and it serves as the combustion chamber in which fuel is fed from the top. It is a batch fed stove in which fuel is loaded into the combustion chamber from the top, and thereafter, the top of the fuel bed is ignited. No fuel was added into the combustion chamber during the operation of the stove. The cookstove is equipped with separate primary and secondary air fans that can be operated anywhere between 0-12 volts. The primary and secondary airflow rates were varied in the range of 0-0.005 kg/s. The primary airflow rate was gradually increased to 0.003 kg/s, while the secondary airflow rate was increased to 0.005 kg/s during the start-up phase. The airflow rates in this type of cookstove model can be assumed to be axisymmetric as per the existing literature. Several authors have verified this assumption by modelling the computational models with the comparable geometries (Ali & Wei, 2017, Pundle et al., 2019, Pande et al., 2020). The primary air is supplied to the cookstove via a grate kept at the bottom of the combustion chamber. In contrast, the secondary air is forced to pass through an annulus chamber formed between the inner and outer cylinders. The purpose of this design is to preheat the secondary air, and to prevent the wall of the combustion chamber from getting too hot. The secondary air is introduced into the combustion chamber through two rows of holes located at the chamber's top. The primary and secondary airflow rates are controlled by using a regulated dc voltage supply.

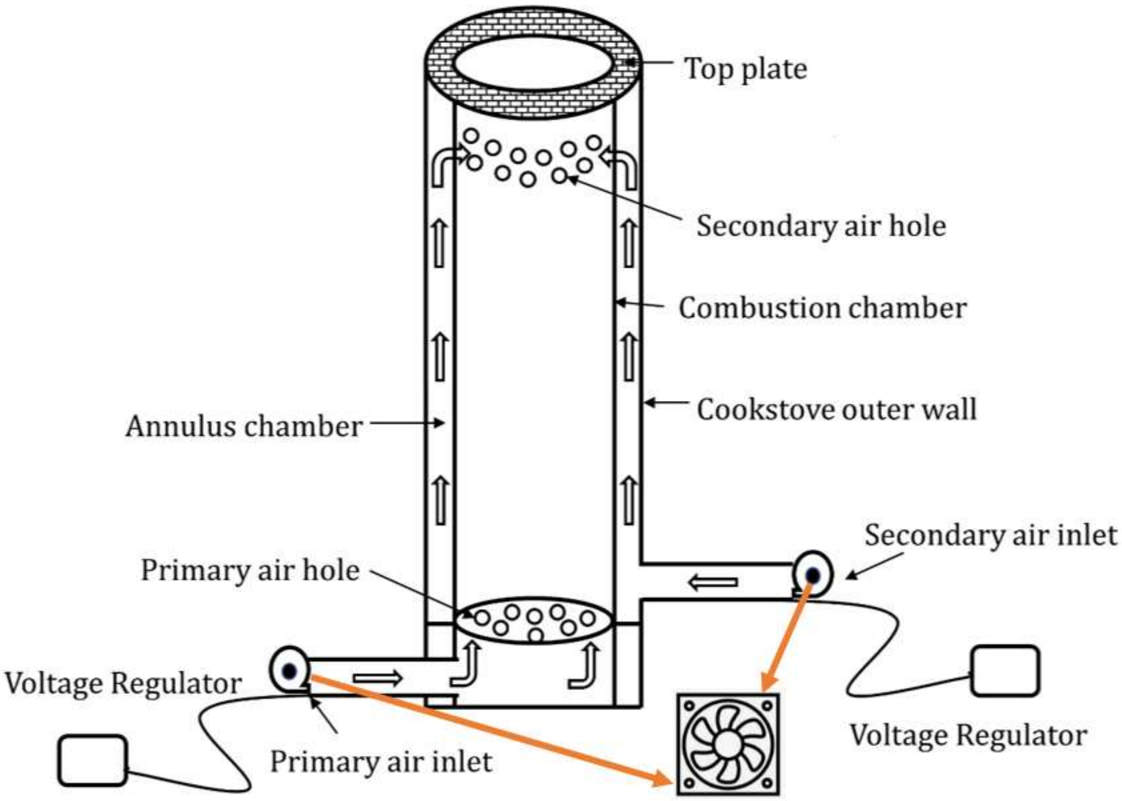

(a)

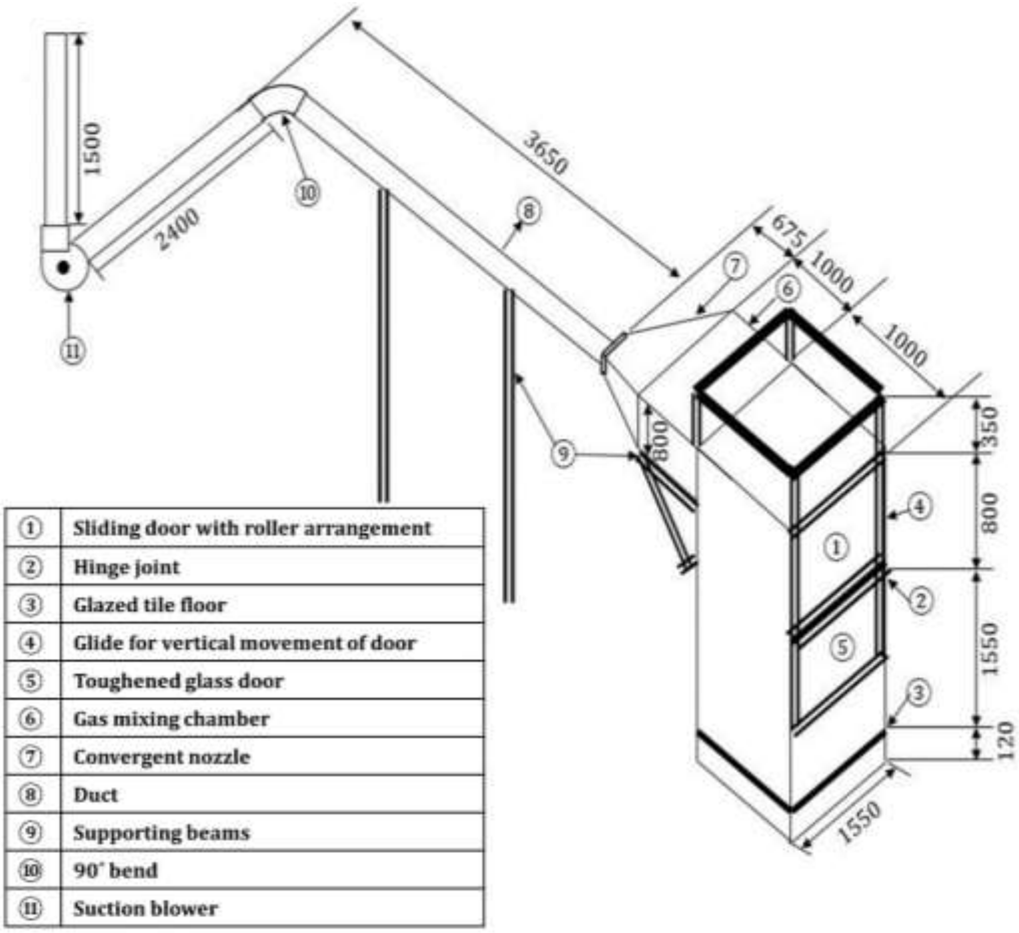

(b)

Fig. 1. Schematic diagram of (a) A forced draft cookstove and (b) An experimental testing facility

2.6 Thermal performance and emission characteristics

The thermal performance and emission characteristics of the cookstove were determined using the experimental testing facility available at the Department of Energy Science and Engineering, IIT Delhi. The schematic of the experimental setup is shown in Fig. 1b. The cookstove was tested for the thermal efficiency and emissions measurement simultaneously, and kept inside the hood to capture the flue gases adequately without affecting the combustion of the cookstove. The hood was closed from all the sides except the front, which had a transparent sliding shutter of toughened glass. The hood was connected with the mixing chamber to dilute the emissions with ambient air homogeneously before sampling. Thereafter, diluted exhaust emissions were forced to pass through the duct via a suction blower installed at the outlet of the duct. The dilution ratio required for the emissions testing was maintained using a variable frequency drive (VFD) (Delta, M02E), which further controlled the speed of the suction blower. The ratio of the average mass flow rate of the diluted exhaust gas in the duct to the average burning rate of the fuel was kept 150:1 during the testing as per the standard protocol (BIS, 2013).

The thermal efficiency of the cookstove was determined by using the water boiling test in the cookstove testing protocols defined by (BIS, 2013). The pellets of 8 mm diameter were used in this study, and the proximate and ultimate analyses are shown in Table 1. A small quantity of ethanol (10 ml) was sprinkled over the fuel bed to initiate the fire. After igniting the fuel bed with a match stick, the primary and secondary air fans were switched on, and speeds were increased gradually according to smoke level, real time CO emission and colour of flame. The cooking pot having a quantity of water, as specified in the testing protocol in accordance with the heat input rate, was kept over the cookstove, and time was recorded. The water temperature in the pot was measured using a PT-100 temperature probe having a resolution of 0.1 ˚C after interval of five minutes, as specified in the protocol. The pot kept over the cookstove was replaced by a second pot having water at ambient temperature, once the temperature in the first pot reached 95 ˚C. The time taken for boiling in each pot was noted down, and the process was repeated until the flame vanished from the combustion chamber. A set of five experiments were repeated to ensure the accuracy of results, and the average values are reported in this manuscript.

Table 1: Proximate and ultimate analysis (as received basis) of pellets

Proximate analysis		**Ultimate analysis**	
Component	**Weight (%)**	**Component**	**Weight (%)**
Moisture content	8.1	Carbon	45.75
Volatile matter	71.9	Oxygen	47.38
Fixed carbon	14.9	Hydrogen	6.65
Ash content	5.1	Nitrogen	0.21
HHV	4136 kcal/kg	Sulphur	0.02

The thermal efficiency and emissions of CO and $PM_{2.5}$ from the cookstove were evaluated using the standard testing methodology described by BIS, while maintaining the temperature of the laboratory at 25±5 ˚C during the experiments (BIS, 2013). The concentration of the CO in the diluted exhaust gas was measured by using a portable gas analyzer (Horiba, PG-350). This multi-component gas analyzer with a built-in sample conditioning and processing unit used the Non-Dispersive Infrared (NDIR) principle to measure CO, CO_2, and SO_2. In contrast, O_2 and NO measurement was based on paramagnetic method and chemiluminescence detection, respectively. The gas analyzer had a wide range of 0-5000 ppm for CO measurement, along with a built-in data logger unit with an SD memory card to facilitate data storage. The resolution of different gases monitored during the experiments is shown in Table 2.

Table 2: Resolution of real time monitoring of gaseous pollutants

S. No.	Gas	Resolution
1.	NO	0.1 ppm
2.	SO_2	0.1 ppm
3.	CO	0.1 ppm
4.	CO_2	0.01 vol%
5.	O_2	0.01 vol%

The emission measurement of fine particulate matter ($PM_{2.5}$) was carried out gravimetrically using a cyclone sampler (URG-2000-30-E-5-2.5-S) having a cut size of 2.5 microns. The diluted exhaust gas was forced to pass through a filter having a pore size of 2 microns at the flow rate of 5 lpm by using a vacuum pump. The sampler flow rate was maintained using a critical orifice and mechanical rotameter, with an operating range of 0-10 lpm. The particulate samples were deposited on polytetrafluoroethylene (PTFE) filters having O ring support. PTFE filters of 47 mm diameter were used in this study due to their hydrophobic nature. The filters were weighed before and after the deposition using a precision weighing balance (METTLER TOLEDO, MS205DU) with a resolution of 10 μg.

2.7 Computational modelling

The computational domain was modelled in ANSYS Fluent to analyse the flow field, and further estimate the heat losses from the forced draft cookstove model designed and fabricated at IIT Delhi. A 2-D axisymmetric geometry was created as shown in Fig. 2 to reduce the complexity and computational time while capturing the important features of the actual cookstove. The complete model was divided into two domains, viz. combustion chamber and annulus chamber, and had three inlets for primary air, secondary air, and fuel, and a single outlet for exhaust gases. The dimensions and position of different features of the computational model were kept equivalent to the actual model, except the actual model did not have a pot skirt. A flat bottom round shaped cooking pot of 420 mm diameter was also modelled at a distance of 30 mm above the combustion chamber. The exhaust gases from the combustion chamber were directed towards the outlet through a gap of 30 mm thickness between the pot sidewall and the skirt. The structured quadrilateral elements have been used in the modelling as it offers better accuracy and less computational time. The wood volatiles were taken as fuel to represent the combustion in the computational model.

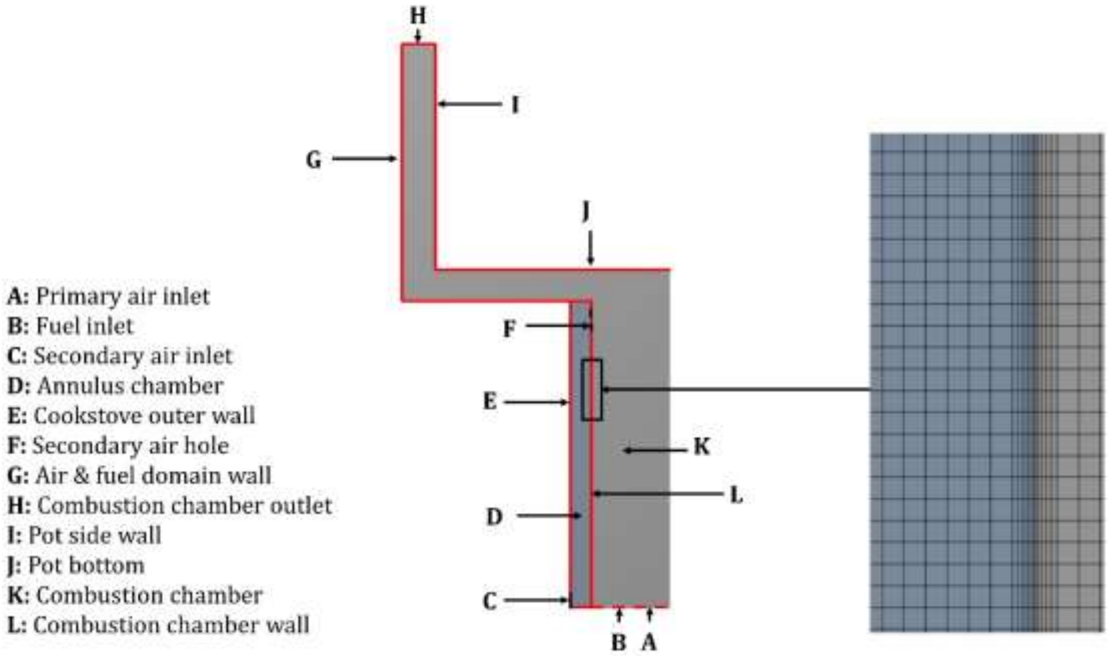

Fig. 2. A 2D axisymmetric computational model

2.7.1 Mathematical model

The primary governing equations of continuity, momentum, and energy were solved in the computational model. Turbulence was modelled using the K-ω SST model as the flow at the top of the combustion chamber was turbulent due to secondary air entrainment. The wall Y plus values were maintained between 0 and 1 to capture the boundary layer effects near the wall. The discrete ordinate method was used to model the radiation in this study (Pundle et al., 2019). The coupled scheme was used for pressure-velocity coupling, while the least square cell-based method discretized the gradient terms. The combustion was modelled using partially premixed combustion in which mass fractions of wood volatiles were specified to model the actual combustion in the simulation (Mitchell et al., 2019, Smith et al., 2020). Diffusion flamelet generated manifold (FGM) model was used as it is preferred for partially premixed turbulent flames that are non-premixed predominantly. Diffusion FGM uses laminar diffusion flame equations transformed from physical space (X) to mixture fraction space (f), where X and f are independent variables. The equations of mixture fraction space for mass fraction species are solved as follows (Fluent, 2017):

$$\rho \frac{\partial Y_i}{\partial t} = \frac{1}{2}\rho X \frac{\partial^2 Y_i}{\partial f^2} + S_i \tag{5}$$

The other equation that is solved for temperature is as follows (Fluent, 2017):

$$\rho \frac{\partial T}{\partial t} = \frac{1}{2}\rho X \frac{\partial^2 T}{\partial f^2} - \frac{1}{C_p}\sum_i H_i S_i + \frac{1}{2C_p}\rho X \left[\frac{\partial C_p}{\partial f} + \sum_i C_{p,i}\frac{\partial Y_i}{\partial f}\right]\frac{\partial T}{\partial f} \tag{6}$$

Where Y_i is the mass fraction for i^{th} species; ρ is density; T is temperature; f is mixture fraction; $C_{p,i}$ is species specific heat for i^{th} iteration; C_p is the average specific heat of mixture; H_i and S_i are specific enthalpy and species reaction rate for i^{th} species, respectively. Scalar dissipation X across the flamelet is modelled by using the following equation (Fluent, 2017):

$$X(f) = \frac{a_s}{4\pi}\frac{3\left(\sqrt{\rho_\infty/\rho}+1\right)^2}{2\sqrt{\rho_\infty/\rho}+1} exp(-2[erfc^{-1}(2f)]^2) \tag{7}$$

where, a_s is characteristic strain rate; ρ_∞ is the density of oxidizer stream; $erfc^{-1}$ is the inverse complementary error function. Diffusion FGMs are calculated from steady diffusion laminar flamelets by transforming the flamelet species field to reaction progress variable (c), the normalized fraction of product species ($c = \frac{Y_c}{Y_c^{eq}}$). The transport equation is solved corresponding to the un-normalized progress variable (Y_c) for FGM turbulent closure as follows (Fluent, 2017):

$$\frac{\partial(\rho\widetilde{Y_c})}{\partial t} + \nabla\left(\rho\vec{v}\widetilde{Y_c}\right) = \nabla\left[\left(\frac{K}{C_p} + \frac{\mu_t}{Sc_t}\right)\nabla\widetilde{Y_c}\right] + \overline{S_{Yc}} \tag{8}$$

where, K is the laminar thermal conductivity of the mixture; C_p is the specific heat of mixture; Sc_t is the turbulent Schmidt number, μ_t is turbulent viscosity of mixture. $\overline{S_{Yc}}$ is the mean source term and can be calculated by using the following equation (Fluent, 2017):

$$\overline{S_{Yc}} = \bar{\rho}\iint S_{FR,Yc}(c,f)P(c,f)dcdf = \overline{S_{FR}} \tag{9}$$

Where S_{FR} is the finite rate flamelet source term; P is the joint probability density function (PDF) of reaction progress I and mixture fraction (f). The above reaction contains the product of two beta PDFs and hence requires second moments i.e. variance. The transport equation used for calculation of the variance of un-normalized reaction progress variable is as follows (Fluent, 2017):

$$\frac{\partial\left(\rho\widetilde{Y_c''}^2\right)}{\partial t} + \nabla\left(\rho\vec{v}\widetilde{Y_c''}^2\right) = \nabla\left[\left(\frac{K}{C_p} + \frac{\mu_t}{Sc_t}\right)\nabla\widetilde{Y_c''}^2\right] + C_\varphi\frac{\mu_t}{Sc_t}\left|\nabla\widetilde{Y}_c\right|^2 - \frac{\rho C_\varphi \widetilde{Y_c''}^2}{\tau_{turb}} \tag{10}$$

where, C_φ is 2.

2.7.2 Boundary conditions

It is essential to use appropriate boundary conditions to get appropriate results. The inlet area ratios of the computational model were kept similar to the experimental model. Mass flow inlet boundary conditions were assigned for both air and fuel inlets. The air was assumed to be entering at 300 K with 23.2% oxygen and 76.8% nitrogen by weight. The mass flow rate of the fuel at the inlet was assigned according to the burning rate of the cookstove obtained from the actual experimental results. The fuel at the inlet was assumed to be a mixture of wood volatiles and mass fractions of the various components (Cassidy, 2020). The outermost wall of the cookstove and pot skirt were assigned a convective heat transfer coefficient of 10 W/m^2-K with the no-slip condition, while assuming the free stream temperature to be 300 K (Cassidy, 2020). The temperature of the cooking pot of the cookstove was maintained at 373 K, which is equivalent to the saturation temperature of water at atmospheric pressure. The pressure outlet condition was assigned at the outlet of the cookstove with atmospheric pressure conditions.

2.7.3 Grid independent test

Meshing has been done in ANSYS Mesher with quadrilateral elements. An inflation layer was applied to generate prism elements to capture the temperature gradients near the boundary layer. Grid independent test has been carried out by varying the mesh size to ensure the accuracy of computational results. The wall heat flux at the vessel's bottom has been plotted with four mesh sizes ranging from 0.4 mm – 2.0 mm as shown in Fig. 3. The preliminary simulations indicated that the mesh size of 0.5 mm is sufficient to run the simulations. There is only a marginal difference between the heat flux values when simulations were performed with a mesh size of less than 0.5 mm, as shown in Fig. 3.

Therefore, a mesh size of 0.5 mm was selected in the present study to save computational time while ensuring reliable results.

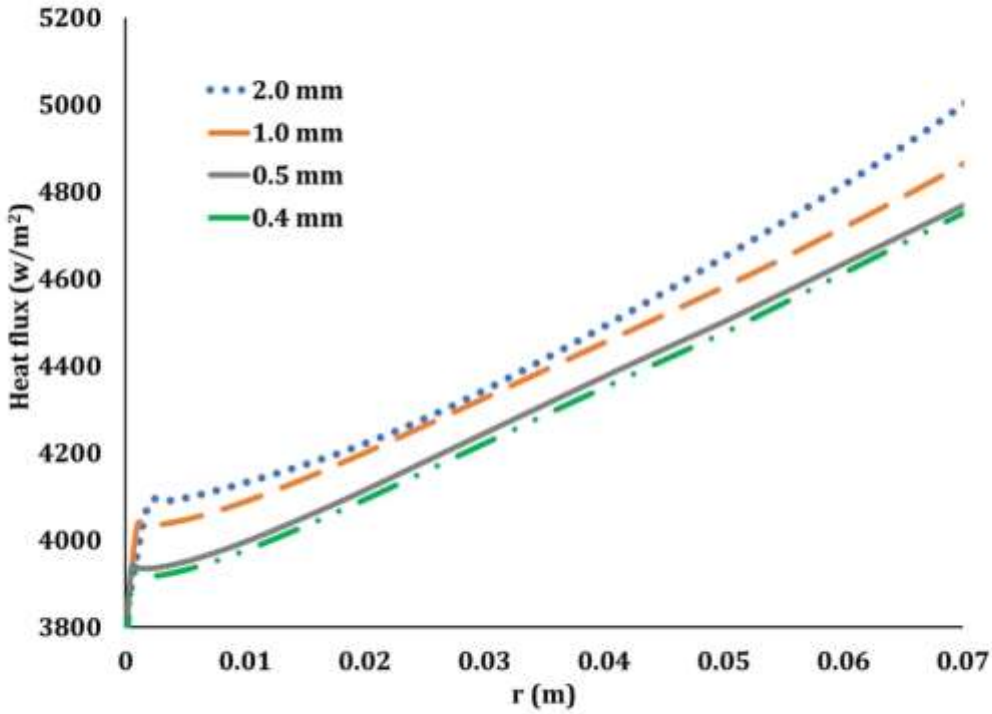

Fig. 3. Variation of wall heat flux on the bottom of the vessel

2.7.4 Model validation

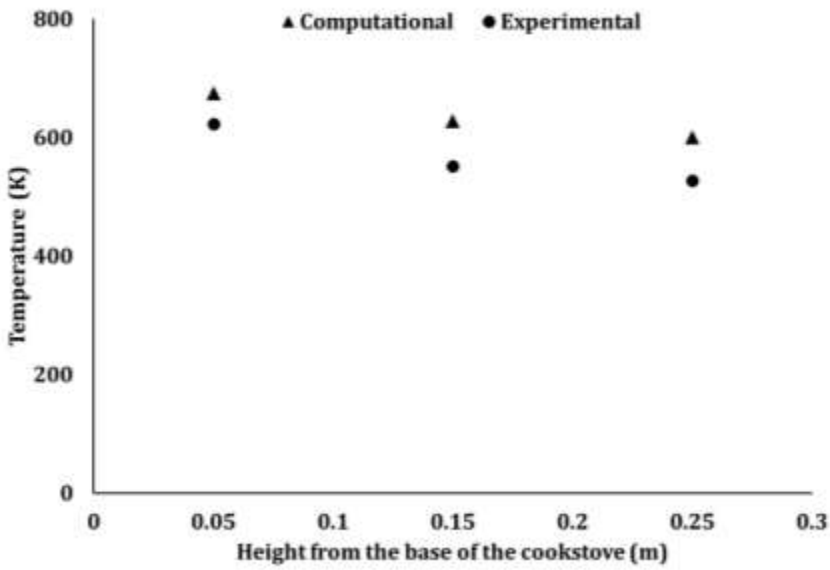

Fig. 4. Variation of outer wall temperature with height from the base of the cookstove

The computational results have been validated with the experimental results acquired from the testing of the developed model and are in good agreement. The highest flame temperature at the top portion of the cookstove obtained from computational and experimental results was 1108 K and 1060 K, respectively. The percentage difference between the experimental and computational values of flame temperature was 4.5%, which is within acceptable limits. The variation of temperature of outer wall with height from the base of the cookstove is shown in Fig. 4, and the values obtained from computational and experimental study are found to be in good agreement. Also, the thermal efficiency obtained from the computational results was validated with the experimental values. The computational and experimental values of the thermal efficiency were found to be 41.48% and 41.34%, respectively, and seem to be in agreement.

3 Uncertainty analysis

The uncertainty analysis was carried out to ensure the accuracy of the experimental results. The analysis included both random and systematic uncertainties that occurred during the different activities such as weighing filters, water, fuel, pot; and measurement of temperature, velocity, and CO concentration during the experiments. The uncertainty in Q, which is a function of a number of independent variables $x_1, x_2, x_3, \ldots, x_n$ having $u_1, u_2, u_3, \ldots, u_n$ as their corresponding uncertainties can be evaluated by using the following relation (Holman, 2012):

$$U_Q = \left[\left(\frac{\partial Q}{\partial x_1}u_1\right)^2 + \left(\frac{\partial Q}{\partial x_2}u_2\right)^2 + \left(\frac{\partial Q}{\partial x_3}u_3\right)^2 + \ldots\ldots\ldots\ldots\ldots\ldots\ldots + \left(\frac{\partial Q}{\partial x_n}u_n\right)^2\right]^{\frac{1}{2}} \quad (11)$$

The uncertainties were calculated using the resolution of different measuring instruments used during data collection and the uncertainties associated with each piece of equipment. The uncertainties involved in calculating thermal efficiency, CO emissions and $PM_{2.5}$ emissions were found to be in the range of 0.9% - 2.9%, 1.2% - 2.5% and 1.2% - 2.5%, respectively.

4 Results and discussions

The primary and secondary airflow rates were governed using a dual supply dc voltage regulator that could supply the voltage in the range of 0 – 30 volts. The airflow rates were optimized by performing several experimental trials, while monitoring the combustion zone temperature at the top of the cookstove. The higher combustion zone temperature led to more complete burning of the volatiles released during gasification and hence, resulted in the lower emission of pollutants. Therefore, the primary and secondary airflow rates were regulated in the present study to obtain the maximum combustion zone temperature. The variation of combustion zone temperature at the top of the combustion chamber and CO concentration with the operating time of the cookstove is shown in Fig. 5. The primary air fan was operated at an airflow rate of 0.002 kg/s, while the secondary air fan was kept off as no volatiles existed during that period. As soon as volatile formation started, the primary and secondary airflow rates were increased gradually to 0.003 kg/s and 0.005 kg/s, respectively, within the first 300 s of the operation of the cookstove, and then the combustion zone temperature also started to rise. Relatively small fluctuations in the combustion zone temperature were observed between the time period of 1000 – 3000 s. The flame front in the fuel bed was continuously moving downward during fuel burning, while the airflow rates were constant during that duration.

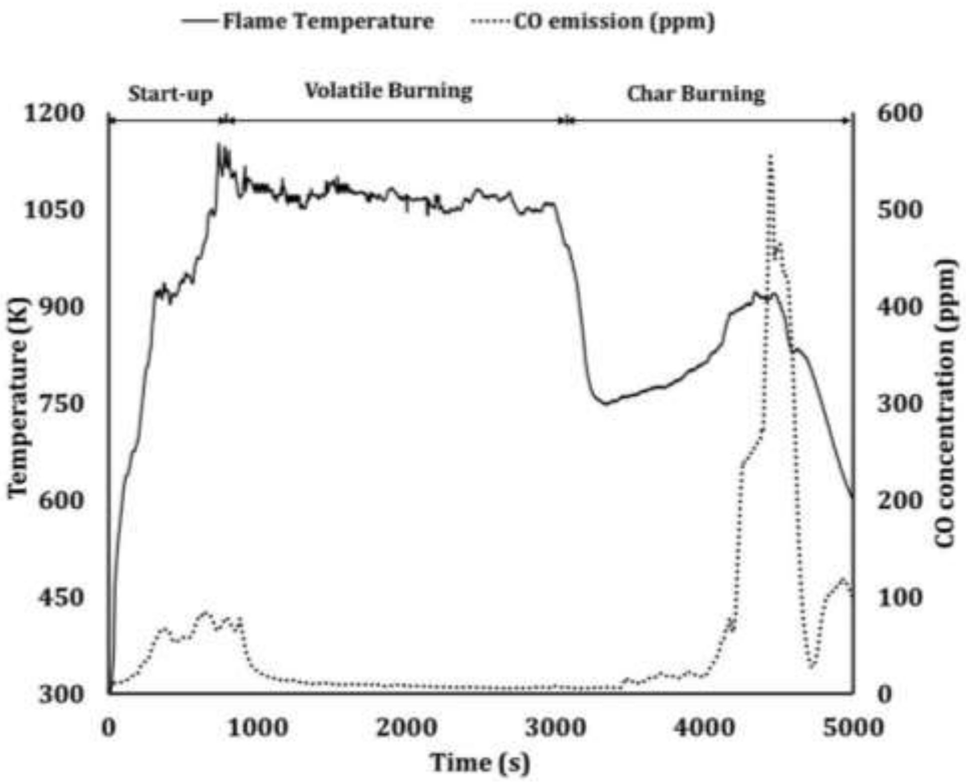

Fig. 5. Variation of combustion zone temperature and CO concentration during the cookstove operation

The average combustion zone temperature of around 1060 K was observed during the volatile burning period, which accounted for most of the energy production during the operation of the cookstove. After volatile burning, the combustion zone temperature started to decline, and the emissions of CO climbed up. Therefore, the secondary airflow rate was decreased gradually to 0.004 kg/s after 3000 s of the cookstove operation. This sharp dip in combustion zone temperature, and the increment in the emissions of CO indicated the beginning of the char burning stage (Tryner et al., 2016). The primary and secondary airflow rates were reduced in the char burning phase as the volatiles vanished out in this stage, and only fixed carbon left in the combustion chamber was burnt. Hence, combustion zone temperature also climbed up as soon as the airflow rates were governed to maximize the combustion zone temperature. During the end of the cookstove operation, as most of the fuel burnt out, the combustion zone temperature dipped sharply. Therefore, the primary and secondary airflow rates were further reduced to 0.002 kg/s after 4500 s of the cookstove operation. The fans were switched off towards the end as flame vanished out in the combustion chamber. Therefore, it is important to govern the airflow rates during the cookstove operation as both the primary air and secondary air significantly affect the temperature of the combustion zone and hence, the thermal efficiency and the emissions of pollutants.

It is clearly visible from Fig. 5 that the combustion can be assumed to be steady in the volatile burning phase as the combustion temperature and concentration of CO were relatively stable. Also, approximately 80% of the total useful heat is delivered to the cooking pot in the volatile burning phase. Numerous studies also indicated that the volatile burning phase in these types of cookstove can assumed to be steady state, and also accounts for the majority of the cookstove operation time (Patel et al., 2016, Pundle et al., 2019, Pande et al., 2020). The average combustion zone temperature at the top of the combustion chamber was around 1060 K from approximately 1000 s to 3000 s during the cookstove operation, as shown in Fig. 5. Therefore, it is important to quantify the heat losses from the forced draft cookstoves to improve the thermal efficiency further. The heat losses from the forced draft gasifier stove have been estimated in this study by modelling the developed cookstove in ANSYS Fluent (MacCarty and Bryden, 2015, Pundle et al., 2019, Pande et al., 2020). The fluid flow and temperature distribution in the combustion chamber and annulus chamber are shown in Fig. 6a-b with the help of contours obtained from the simulations. It can be seen from Fig. 6a that the velocity of the secondary air being introduced into the combustion chamber was found to be in the range of 2.7 – 3.2 m/s. The fluid flow pattern at the top of the cookstove represented that the hot flue gases would contact the vessel's bottom, while moving out of the combustion chamber after the burning of volatiles.

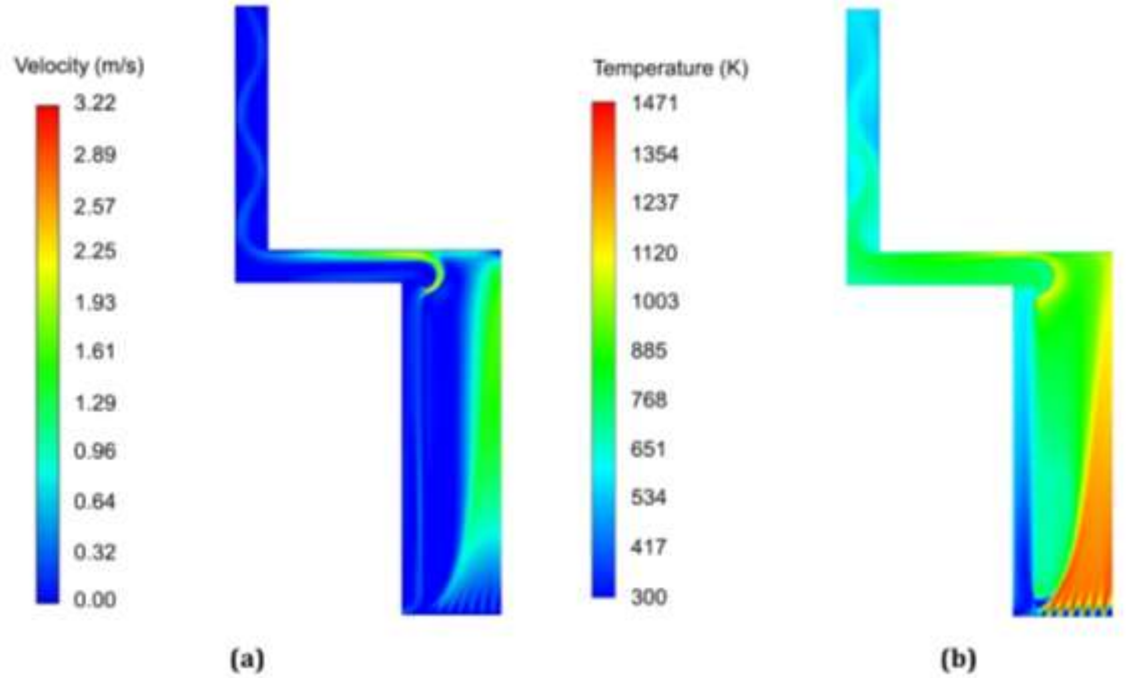

Fig. 6. Contours of (a) Velocity and (b) Temperature distribution in the computational domain

The static temperature distribution across the different domains obtained from the simulation is shown in Fig. 6b. The temperature distribution over the cookstove domain varied between 300 – 1470 K, and the combustion zone temperature at the top of the cookstove was found to be in the range of 935 – 1114 K. The secondary air was preheated up to the temperature of 577 – 600 K before being entering in the combustion chamber, while a significant amount of heat was carried away by flue gas as the temperature near the combustion chamber outlet varied in the range of 577 – 637 K. It can be seen from Fig. 6(a) that the injected secondary air does not penetrate to the center of the combustion chamber, which further suggests that design changes to increase penetration may further improve performance. It is visible from Fig. 6b that the preheated secondary air leaving the secondary air holes created sufficient turbulence leading to homogeneous mixing of volatiles with air, and hence resulting in the nearly complete burning of volatiles. Thus, the improved combustion characteristics lowered the emissions of harmful pollutants which are hazardous for human health and the environment (Zhang and Smith, 2017, Smith et al., 2014).

The variation of temperature and heat flux at the outermost wall of the cookstove with the height is shown in Fig. 7. The heat flux at the outer wall of the cookstove was found to be in the range of 1110 – 4355 W/m^2, while the temperature of the outermost wall range between 400 – 700 K. However, the maximum temperature of the secondary air in the annulus chamber was found to be 637 K. Thus, the temperature of the outer wall of the cookstove was found to be higher than the temperature of secondary air being preheated in the annulus chamber. Therefore, it is clear that the heat transfer from the combustion chamber to the outer wall is predominant via conduction through the top plate covering the annulus chamber and via radiation compared to the convection through the secondary air. The reason for significant heat transfer via conduction could be metal to metal contact of the top plate with the inner and outer wall of the combustion chamber (Sedighi and Salarian, 2017).

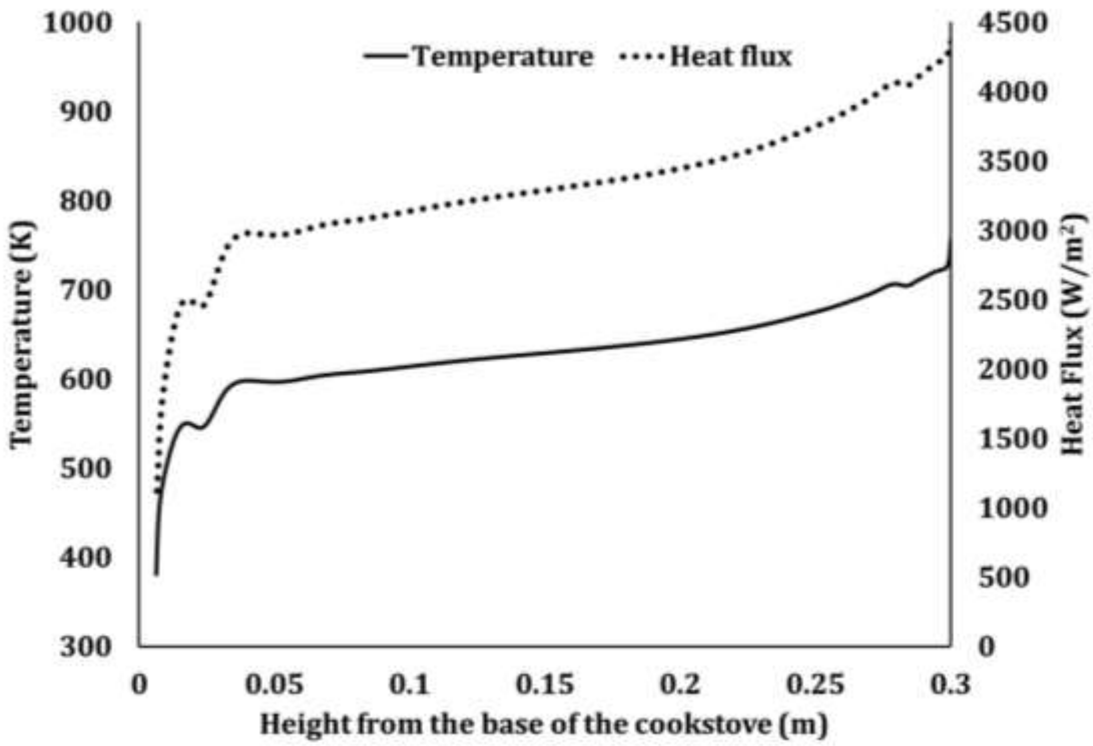

Fig. 7. Variation of temperature and heat flux over the outermost wall of the cookstove

The energy flow diagram of the cookstove representing the percentage of energy being lost from different segments and the useful energy delivered to the cooking pot is shown in Fig. 8. It can be seen from Fig. 8 that more than ¼ of the total energy produced by the burning of fuel is being lost to the atmosphere from the outermost wall of the cookstove. The thermal efficiency of the cookstove, as estimated through the simulation results, was found to be 41.5%, while the energy lost in the flue gas was approximately 17.9%. The total energy lost to the ambient via cooking pot and cookstove bottom were 8.4% and 3.6%, respectively. Therefore, it is important to minimize the heat loss from the outermost wall of the cookstove as well as heat loss in the flue gas further to improve the thermal efficiency of the gasifier stoves, as these losses account for 46.42% of the total energy that is produced by the burning of fuel.

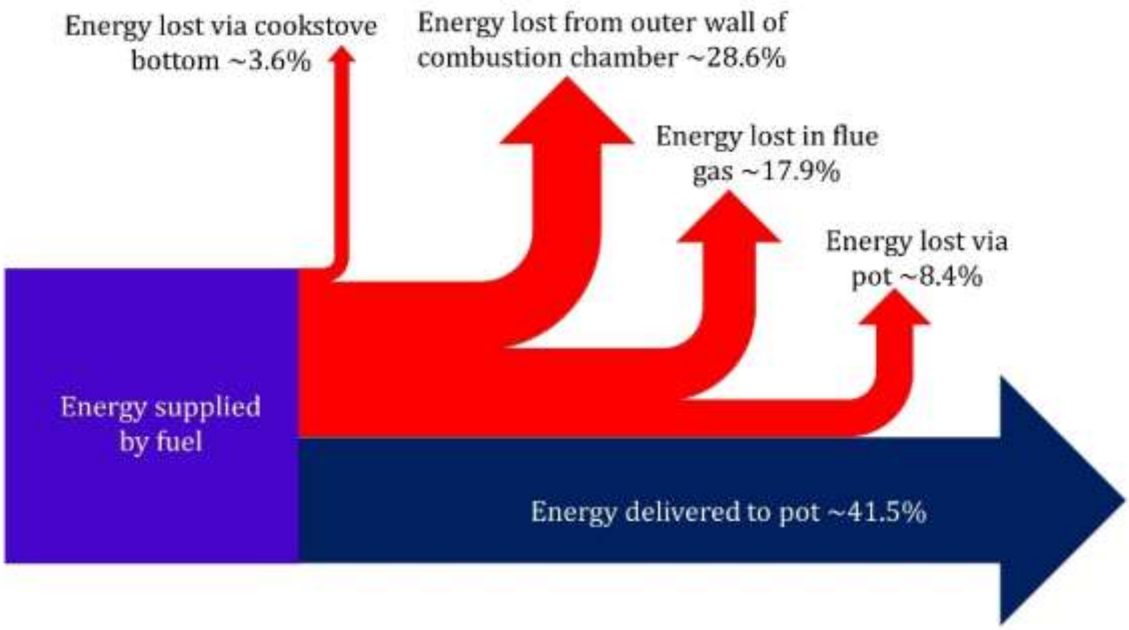

Fig. 8. Estimation of heat loss from forced draft cookstove

The preliminary experimental investigations and computational results revealed that a significant amount of heat was being lost to the ambient from the outermost wall of the developed cookstove FD 2.1. Therefore, the outer wall of the cookstove was insulated by using glass wool of 25 mm thickness to minimize the heat losses, and the cookstove with insulation is referred to as FD 2.2 in this study. The thermal performance and emission characteristics of the FD 2.1 and FD 2.2 models are shown in Fig. 9. The thermal efficiency of the FD 2.1 was found to be around 41.3%, while the emissions of CO and $PM_{2.5}$ per megajoule of useful energy delivered to the cooking vessel (MJ_D) were found to be around 0.98 g/MJ_D and 38.91 mg/MJ_D, respectively. An improvement of 5.7% in the thermal efficiency of the FD 2.2 was attributed to the lesser heat losses from the outermost wall of the cookstove. Further, the reduced heat losses resulted in higher values of combustion zone temperature, and the improvement in efficiency resulted in less fuel consumption for the same amount of useful energy, further leading to reduced emissions on a useful energy basis. Therefore, the emissions of CO and $PM_{2.5}$ from the FD 2.2 were decreased by 7.1% and 25.8%, respectively, due to increased combustion zone temperature leading to more complete combustion of volatiles.

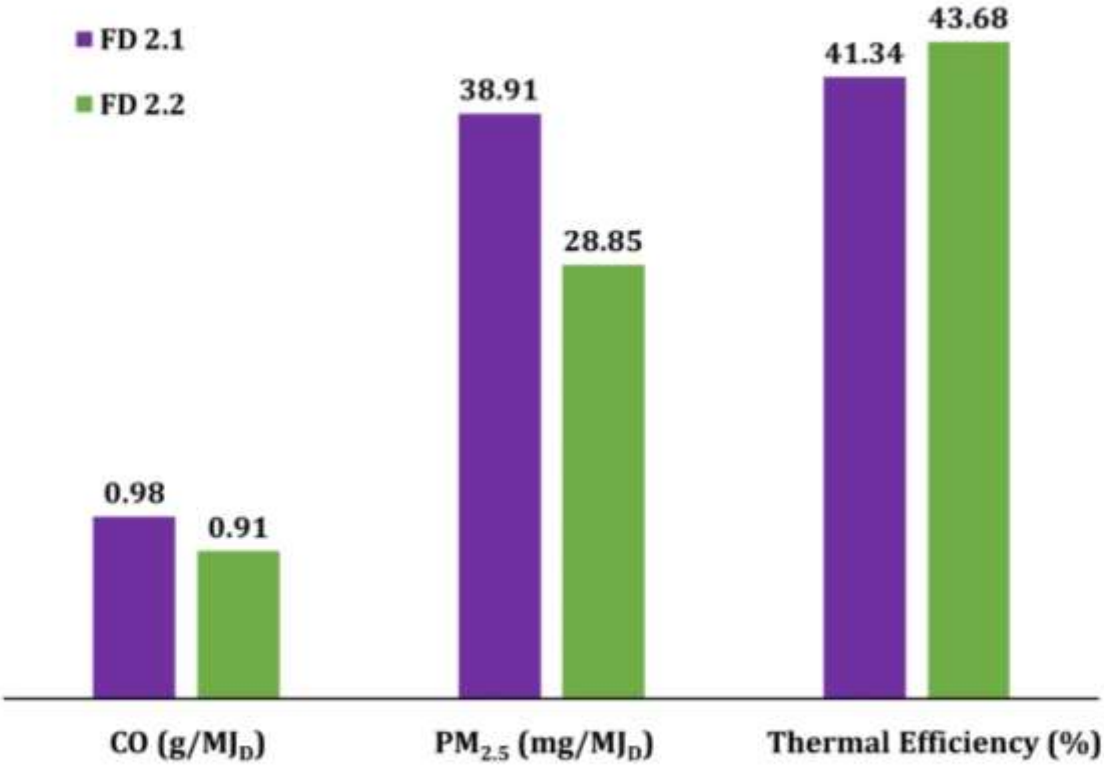

Fig. 9. Comparison of thermal efficiency and emissions of CO and $PM_{2.5}$ from FD 2.1 and FD 2.2 cookstove models

The comparison of the thermal performance and emission characteristics of the models developed in the present study has also been carried out with other forced draft cookstove models tested following standard protocols as shown in Figs. 10a-b (CCA, 2013). It must be noted that other forced-draft stoves were tested with different protocols, so the comparison is not exact. However, the objective of this study is to compare the performance of developed models with other forced draft models available worldwide, while utilizing pellets as fuel. BIS adopts a methodology which quantitatively measures the emissions of CO and $PM_{2.5}$, and most of the parameters and procedures given in the newly developed methodology like International Organization for Standardization (ISO) are similar to the BIS standards, while operating in high power mode (ISO, 2018). Therefore, according to BIS or ISO methodology, CO, $PM_{2.5}$ and thermal efficiency are the important performance parameters for any cookstove. Also, emissions are calculated per unit useful energy delivered to the cooking vessels during different protocols in high power mode, and hence, can be compared.

The mode of primary and secondary air supply in the developed models differed from the other models in this study (CCA, 2013). The developed models viz. FD 2.1 and FD 2.2 were equipped with individual primary and secondary air fans which assisted in the precise control over the airflow rates, while the other models had a single fan. Therefore, the required airflow rate ratios of primary and secondary air were maintained as per the requirement during the different phases of combustion throughout the cookstove operation. It can be seen from Fig. 10a that the thermal efficiency of the Mimi moto cookstove model was found to be highest, followed by FD 2.2, ACE 1, FD 2.1, Philips HD4012, Elegance 2015 and Oorja cookstove.

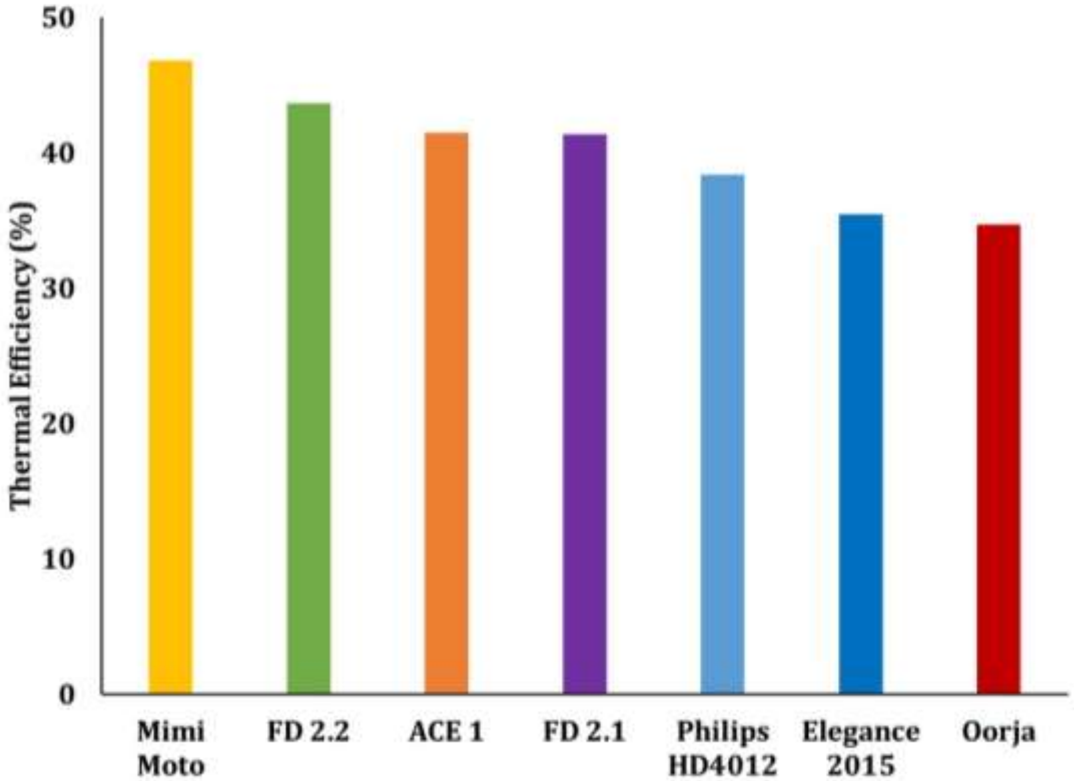

(a)

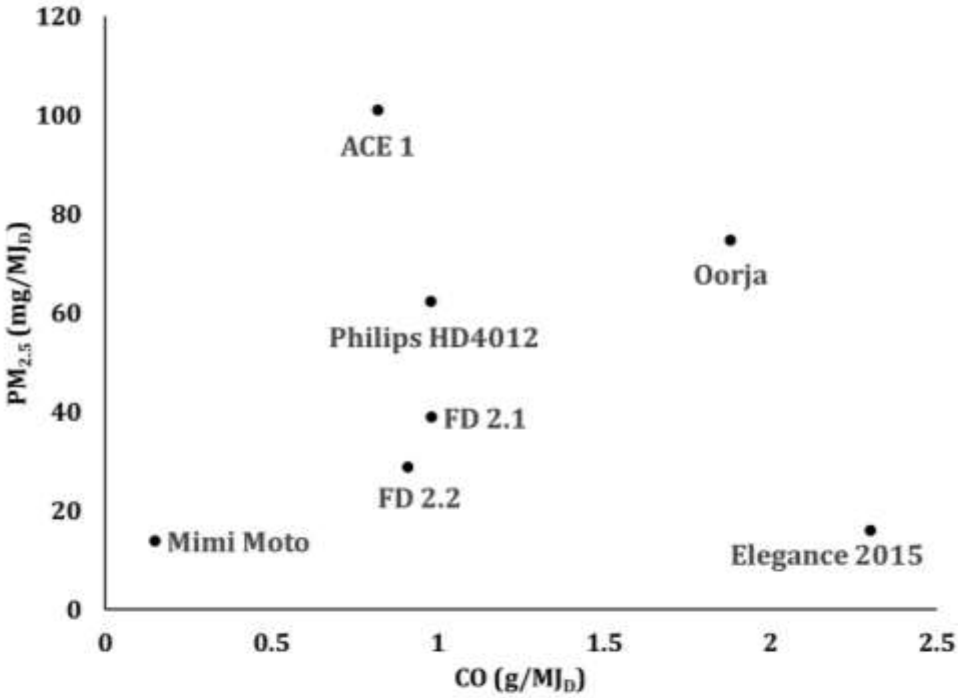

(b)

Fig. 10. Comparison of (a) Thermal efficiency and (b) Emissions of CO and $PM_{2.5}$ with other forced draft pellet based cookstoves

The emissions of CO and $PM_{2.5}$ for different cookstoves have been plotted as shown in Fig. 10b. The comparison is not exact as other forced draft cookstove models were tested using different protocols. It is visible from Fig. 10b that the emission of CO from FD 2.1, FD 2.2, Philips HD4012 and ACE 1 stove is similar, while the emission of $PM_{2.5}$ from FD 2.2 is significantly lower than the other stoves except Mimi Moto and Elegance 2015. The Mimi Moto cookstove exhibited the least emissions of CO and $PM_{2.5}$ The emission of $PM_{2.5}$ from the Elegant 2015 model is 0.55 times lower than the FD 2.2 cookstove; however, the emission of CO was 2.5 times higher. Also, the thermal efficiency of the FD 2.2 cookstove model was 23.25% higher than that of the Elegance 2015 cookstove. Therefore, the FD 2.2 model seems to be the most efficient, except for the Mimi Moto if all three performance parameters, viz. thermal efficiency, emissions of CO and $PM_{2.5}$ are considered. The higher thermal efficiency and lower emissions of both CO and $PM_{2.5}$ from the FD 2.2 model were attributed to the different primary and secondary air fans, which assisted the governing of airflow rates during the operation of the cookstove.

The precise control over the airflow rates and insulation layer on the outer wall of the FD 2.2 model resulted in the higher combustion zone temperatures, which further led to the nearly complete burning of volatiles released during gasification. The higher cost of production due to separate controls may be compensated by the reduction of harmful pollutants which is directly linked to human health. Further, we are working on automation of air supply for smooth operation in order to regulate airflow rates automatically without end user's intervention.

The cookstoves developed in the present work uses densified fuel pellets, and these pellets can be made from crop residues, which are abundantly available and otherwise burnt in the open fields leading to emission of huge amount of pollutants. In 2017, crop residue burning added 824 Gg of $PM_{2.5}$, 812 Gg of PM_{10}, 58 Gg of Elemental Carbon (EC) and 239 Gg of Organic Carbon (OC) in India (Ravindra et al., 2019). These emissions can be minimized by using these crop residues as feedstock material for production of pellets, which may be further combusted efficiently in improved cookstoves as developed in the present work. Therefore, these crop residues have huge potential to fulfil the thermal energy requirement of domestic cooking, if burnt properly. In this way, the emission of pollutants from stubble burning and traditional cookstoves using different solid fuels can be minimized.

5 Conclusions

The present article represented the experimental and computational studies of a forced draft biomass pellet based cookstove (FD 2.1) having separate primary and secondary air supplies. The airflow rates were controlled precisely during the different phases of combustion to obtain the higher combustion zone temperatures, resulting in improved thermal efficiency and reduced emissions of pollutants. FD 2.1 was further insulated by using glass wool, and the modified model termed FD 2.2 showed an improvement in the thermal efficiency and emission characteristics. The thermal efficiency of FD 2.2 was found to be highest as compared to the other forced draft cookstove models, except for the Mimi Moto. The performance of the FD 2.1 cookstove has also been analysed through computational modelling, and the simulation results indicated that the heat loss from the combustion chamber to the outer wall is predominant via conduction through the top plate of the cookstove and via radiation as compared to the convection through preheated secondary air in the combustion chamber. Also, it was found that around 46.4% of the total energy produced by the burning of fuel was being lost to the environment through the outermost wall and flue gas.

Acknowledgments

Sincere thanks are due to IIT Delhi for providing the assistance to set-up the laboratory facilities for the academic and R&D activities at Department of Energy Science and Engineering. One of the authors (Himanshu) is thankful to Prof. K. K. Agrawal, Mech. Engg. Deptt. IIT Delhi for technical discussions in computational modelling. This work is also dedicated to Late Prof. K. R. Smith for fruitful discussions on emission measurements during his visit to IITD in the year 2018.

References

Ali, H., Wei, T.T.J., 2017. CFD study of an improved biomass cookstove with reduced emission and improved heat transfer characteristics. J. Clean Energy Technol. 5(6), 427-432. https://doi.org/10.18178/jocet.2017.5.6.410.

Arora, P. and Jain, S., 2016. A review of chronological development in cookstove assessment methods: Challenges and way forward. Renew. Sust. Energ. Rev. 55, pp.203-220. https://doi.org/10.1016/j.rser.2015.10.142.

Belonio, A.T., 2005. Rice husk gas stove handbook. Iloilo City, Philippines: Central Philippine University.

Birzer, C., Medwell, P., Wilkey, J., West, T., Higgins, M., Macfarlane, G., Read, M., 2013. An analysis of combustion from a top-lit up-draft (TLUD) cookstove. J. Humanit. Eng. 2(1), 1-8. https://doi.org/10.36479/jhe.v2i1.11.

Bonjour, S., Adair-Rohani, H., Wolf, J., Bruce, N.G., Mehta, S., Prüss-Ustün, A., Lahiff, M., Rehfuess, E.A., Mishra, V., Smith, K.R., 2013. Solid fuel use for household cooking: country and regional estimates for 1980–2010. Environ. Health Perspect. 121(7), 784-790. https://doi.org/10.1289/ehp.1205987.

Bureau of Indian Standards, 2013. Indian standard on Portable Solid Biomass Cookstove (Chulha First Revision). IS 13152 (Part 1).

Cassidy, L.J., 2020. Advancing forced draft biomass cookstove technology with computational fluid dynamics modeling. https://ir.library.oregonstate.edu/concern/graduate_thesis_or_dissertations/1g05fj85j. (Accessed 15 March 2021)

Caubel, J.J., Rapp, V.H., Chen, S.S., Gadgil, A.J., 2018. Optimization of secondary air injection in a wood-burning cookstove: an experimental study. Environ. Sci. Technol. 52(7), 4449-4456. https://doi.org/10.1021/acs.est.7b05277.

Caubel, J.J., Rapp, V.H., Chen, S.S. and Gadgil, A.J., 2020. Practical design considerations for secondary air injection in wood-burning cookstoves: An experimental study. Dev. Eng. 5, p.100049. https://doi.org/10.1016/j.deveng.2020.100049.

Chen, Y., Shen, G., Su, S., Du, W., Huangfu, Y., Liu, G., Wang, X., Xing, B., Smith, K.R., Tao, S., 2016. Efficiencies and pollutant emissions from forced-draft biomass-pellet semi-gasifier stoves: Comparison of International and Chinese water boiling test protocols. Energy Sustain Dev., 32, 22-30. https://doi.org/10.1016/j.esd.2016.02.008.

Chendake, A.D., Shelake, P.S., Nalawade, R.D., Vairal, S.D., 2014. Design and development of household gasifier cum water heater. Int J Curr Eng Technol. ISSN, 2277-4106.

Clean Cooking Alliance, 2022. Clean cooking catalog. http://catalog.cleancookstoves.org/stoves (Accessed 05 May 2022)

Fluent, A.N.S.Y.S., 2017. ANSYS Fluent theory guide 18.0. Ansys Inc.

Gupta, A., Mulukutla, A.N., Gautam, S., TaneKhan, W., Waghmare, S.S., Labhasetwar, N.K., 2020. Development of a practical evaluation approach of a typical biomass cookstove. Environ. Technol. Innov., 17, 100613. https://doi.org/10.1016/j.eti.2020.100613.

Himanshu, H., Pal, K., Jain, S., Tyagi, S. K., 2021. Development of advanced biomass cookstove and performance comparisons using the modified star rating methodology. Energy Eng. 118(5), 1237–1251. https://doi:10.32604/EE.2021.016489.

Holman, J. P., 2012. Experimental Methods for Engineers, 8th ed., New York, McGraw-Hill.

Husain, Z., Tiwari, S.S., Pandit, A.B., Joshi, J.B., 2019. Computational Fluid Dynamics Study of Biomass Cook Stove—Part 1: Hydrodynamics and Homogeneous Combustion. Ind. Eng. Chem. Res. 59(9), 4161-4176. https://doi.org/10.1021 /acs.iecr.9b03181.

International Energy Agency (IEA), 2020. SDG7: Data and Projections. IEA, Paris. https://www.iea.org/reports/sdg7-data-and-projections. (Accessed 21 March 2022).

International Organization for Standardization, 2018. Clean cookstoves and clean cooking solutions — Harmonized laboratory test protocols — Part 1: Standard test sequence for emissions and performance, safety and durability. ISO 19867-1. https://www.iso.org/standard/66519.html. (Accessed 14 June 2022).

Jetter, J., Zhao, Y., Smith, K.R., Khan, B., Yelverton, T., DeCarlo, P., Hays, M.D., 2012. Pollutant emissions and energy efficiency under controlled conditions for household biomass cookstoves and implications for metrics useful in setting international test standards. Environ. Sci. Technol. 46(19), 10827-10834. https://doi.org/10.1021/es301693f.

Kim, K.H., Jahan, S.A., Kabir, E., 2011. A review of diseases associated with household air pollution due to the use of biomass fuels. J. Hazard. Mater. 192(2), 425-431. https://doi.org/10.1016/j.jhazmat.2011.05.087.

Kirch, T., Birzer, C. H., Eyk, P. J. V., Medwell, 2018. Influence of primary and secondary air supply on gaseous emissions from a small-scale staged solid biomass fuel combustor. Energy Fuels. 32, 4212-4220. https://doi.org/10.1021/acs.energyfuels.7b03152.

Kirch, T., Medwell, P.R., Birzer, C.H., 2016. Natural draft and forced primary air combustion properties of a top-lit up-draft research furnace. Biomass Bioenergy. 91:108-115. https://doi.org/10.1016/j.biombioe.2016.05.003.

MacCarty, N., Still, D., Ogle, D., 2010. Fuel use and emissions performance of fifty cooking stoves in the laboratory and related benchmarks of performance. Energy Sustain. Dev. 14(3), 161-171. https://doi.org/10.1016/j.esd.2010.06.002.

MacCarty, N.A., Bryden, K.M., 2015. Modeling of household biomass cookstoves: A review. Energy Sustain. Dev. 26, 1-13. https://doi.org/10.1016/j.esd.2015. 02.001.

Mitchell, E.J.S., Ting, Y., Allan, J., Lea-Langton, A.R., Spracklen, D.V., McFiggans, G., Coe, H., Routledge, M.N., Williams, A. and Jones, J.M., 2019. Pollutant emissions from improved cookstoves of the type used in sub-Saharan Africa. Combust. Sci. Technol. 192, 1582-1602. https://doi.org/10.1080/00102202.2019.1614922.

Obeng, G.Y., Mensah, E. and Opoku, R., 2021. Fabricators and End-Users of Single-Pot Biomass Stoves: Conceptualizing, Hypothesis and Performance Metrics for Developing Energy Sustainability Framework. Sustainability. 13(13), p. 7098. https://doi.org/10.3390/su13137098.

Pal, K., Jha, M.K., Gera, P., Tyagi, S.K., 2016. Experimental study on the performance evaluation and emission reduction potential of different cookstove models using standard design parameters and testing protocols. Biofuels, 7(4), 313-335. https://doi.org/10.1080/17597269.2015.1135373.

Pande, R.R., Kshirsagar, M.P., Kalamkar, V.R., 2020. Experimental and CFD analysis to study the effect of inlet area ratio in a natural draft biomass cookstove. Environ. Dev. Sustain. 22(3), 1897-1911. https://doi.org/10.1007/s10668-018-0269-x.

Pandey, A., Patel, S., Pervez, S., Tiwari, S., Yadama, G., Chow, J.C., Watson, J.G., Biswas, P., Chakrabarty, R.K., 2017. Aerosol emissions factors from traditional biomass cookstoves in India: insights from field measurements. Atmos. Chem. Phys. 17(22), 13721-13729. https://doi.org/10.5194/acp-17-13721-2017.

Patel, S., Leavey, A., He, S., Fang, J., O'Malley, K. and Biswas, P., 2016. Characterization of gaseous and particulate pollutants from gasification-based improved cookstoves. Energy Sustain. Dev., 32, pp.130-139. https://doi.org/10.1016 /j.esd.2016.02.005.

Pundle, A., Sullivan, B., Means, P., Posner, J.D. and Kramlich, J.C., 2019. Predicting and analyzing the performance of biomass-burning natural draft rocket cookstoves using computational fluid dynamics. Biomass and Bioenergy, 131, p.105402. https://doi.org/10.1016/j.biombioe.2019.105402.

Rajkumar, S., Young, B.N., Clark, M.L., Benka-Coker, M.L., Bachand, A.M., Brook, R.D., Nelson, T.L., Volckens, J., Reynolds, S.J., L'Orange, C., Good, N., 2019. Household air pollution from biomass-burning cookstoves and metabolic syndrome, blood lipid concentrations, and waist circumference in Honduran women: a cross-sectional study. Environ. Res. 170, 46-55. https://doi.org /10.1016/j.envres.2018.12.010.

Rapp, V.H., Caubel, J.J., Wilson, D.L., Gadgil, A.J., 2016. Reducing ultrafine particle emissions using air injection in wood-burning cookstoves. Environ. Sci. Technol. 50(15), 8368-8374. https://doi.org/10.1021/acs.est.6b01333.

Ravindra, K., Singh, T. and Mor, S., 2019. Emissions of air pollutants from primary crop residue burning in India and their mitigation strategies for cleaner emissions. J. Clean. Prod, 208, 261-273. https://doi.org/10.1016/j.jclepro.2018.10.031.

Sedighi, M. and Salarian, H., 2017. A comprehensive review of technical aspects of biomass cookstoves. Renew. Sust. Energ. Rev. 70, pp.656-665. https://doi.org/10.1016/j.rser.2016.11.175.

Sharma, M., Dasappa, S., 2017. Emission reduction potentials of improved cookstoves and their issues in adoption: An Indian outlook. J. Environ. Manage. 204, 442-453. https://doi.org/10.1016/j.jenvman.2017.09.018.

Smith, J.D., Sreedharan, V., Landon, M. and Smith, Z.P., 2020. Advanced design optimization of combustion equipment for biomass combustion. Renew. Energy, 145, 1597-1607. https://doi.org/10.1016/j.renene.2019.07.074.

Smith, K.R., Bruce, N., Balakrishnan, K., Adair-Rohani, H., Balmes, J., Chafe, Z., Dherani, M., Hosgood, H.D., Mehta, S., Pope, D., Rehfuess, E., 2014. Millions dead: how do we know and what does it mean? Methods used in the comparative risk assessment of household air pollution. Annu. Rev. Public Health. 35, 185-206. https://doi.org/10.1146/annurev-publhealth-032013-182356.

Srivastava, L., Goswami, A., Diljun, G.M., Chaudhury, S., 2012. Energy access: Revelations from energy consumption patterns in rural India. Energy Policy, 47, 11-20. https://doi.org/10.1016/j.enpol.2012.03.030.

Tryner, J., Tillotson, J. W., Baumgardner, M. E., Mohr, J. T., Defoort, M. W., Marchese, A. J., 2016. The effects of air flow rates, secondary air inlet geometry, fuel type, and operating mode on the performance of gasifier cookstoves. Environ. Sci. Technol. 50(17), 9754-9763. https://doi.org/10.1021/acs.est.6b00440.

Tryner, J., Volckens, J., Marchese, A. J., 2018. Effects of operational mode on particle size and number emissions from a biomass gasifier cookstove. Aerosol Sci. Technol. 52(1), 87-97. https://doi.org/10.1080/02786826.2017.1380779.

Tryner, J., Willson, B. D., Marchese, A. J., 2014. The effects of fuel type and stove design on emissions and efficiency of natural-draft semi-gasifier biomass cookstoves. Energy Sustain Dev. 23, 99-109. https://doi.org/10.1016/j.esd.2014.07.009.

Tyagi, S. K., 2022. Biomass pellet based combustion devices, Indian Patent No. 397919. (Granted on 27 May 2022).

Zhang, J., Smith, K.R., 2007. Household air pollution from coal and biomass fuels in China: measurements, health impacts, and interventions. Environ. Health Perspect. 115(6), 848-855. https://doi.org/10.1289/ehp.9479.

Nomenclature

AFR	Air flow rate
a_s	Characteristic strain rate
c	Reaction progress variable
CO	Carbon-monoxide
CO_2	Carbon dioxide
C_p	Average specific heat of mixture
C_p	Specific heat of mixture
$C_{p,I}$	Species specific heat for i^{th} iteration
CV_f	Calorific value of fuel
D	Diameter of cookstove
$erfc^{-1}$	Inverse complimentary error function
f	Mixture fraction space
FCR	Fuel consumption rate
FGM	Flamelet generated manifold
H	Height of cookstove
HAP	Household air pollution
H_i	Specific enthalpy for i^{th} species
K	Laminar thermal conductivity of mixture
NO	Nitrogen oxide
O_2	Oxygen
P	Joint PDF of reaction progress
PM	Particulate matter
PTFE	Polytetrafluoroethylene
Q	Function

Q_n	Power output
SA	Stochiometric air
Sc_t	Turbulent Schmidt number
S_{FR}	Finite rate flamelet source term
SGR	Specific gasification rate
S_i	Species reaction rate for i^{th} species
SO_2	Sulphur dioxide
$\overline{S_{Yc}}$	Mean source term
t	Time required for operation of cookstove
T	Temperature
$u_1, u_2,..., u_n$	Uncertainties in $x_1, x_2,..., x_n$
VFD	Variable frequency drive
X	Physical space
$x_1, x_2,.., x_n$	Independent variables
Y_i	Mass fraction for i^{th} species

Greek Symbols

η	Thermal efficiency of cookstove
ε	Equivalence ratio
ρ	Density
ρ_f	Density of fuel
ρ_a	Density of air
ρ_∞	Density of oxidizer stream
μ_t	Turbulent viscosity of mixture